C. R. Mecanique 341 (2013) 592–604

Contents lists available at SciVerse ScienceDirect

Comptes Rendus Mecanique

www.sciencedirect.com

Non-linear creep modeling of short-fiber composites using Hermite polynomials, hyperbolic trigonometric functions and power series

Mehdi Mondali [a], Vahid Monfared [b,*], Ali Abedian [c]

[a] Department of Mechanical and Aerospace Engineering, Science and Research Branch, Islamic Azad University, Tehran, Iran
[b] Department of Mechanical Engineering, Zanjan Branch, Islamic Azad University, Zanjan, Iran
[c] Department of Aerospace Engineering, Sharif University of Technology, Tehran, Iran

ARTICLE INFO

Article history:
Received 6 November 2012
Accepted after revision 25 April 2013
Available online 6 June 2013

Keywords:
Steady-state creep
Short-fiber composite
Hermite polynomials
Hyperbolic trigonometric functions
Power series
FEM

ABSTRACT

A novel analytical model is presented for analyzing the steady-state creep in short-fiber composites under axial load utilizing the previous shear-lag theory, the imaginary fiber technique and also new approaches of Hermite polynomials, hyperbolic trigonometric functions and power series. The steady-state creep behavior of the matrix is described by an exponential law, while the fibers behave elastically. In this model, in spite of the previous researches, some unknowns such as shear stress, displacement rates, and creep strain rates are correctly determined in all regions of the unit cell without using any further assumptions. In comparison with previous analytical approaches, the results of the present work are closer to the FEM simulations. This strong method can be used in various problems in applied physics and mechanics such as elastic and plastic analysis of nano-composites.

1. Introduction

The development of advanced aerospace materials depends on their ability to retain stiffness and strength at high temperatures. Metal matrix composites (MMCs) have several advantages such as high strength, high modulus and good conductivities due to the combination of metallic properties such as ductility, toughness, and environmental resistance with ceramic properties such as high strength and modulus. In recent years, the high-temperature creep behavior of SiC whiskers reinforced aluminum alloys has been the subject of studies that aimed at assessing the potential of these composites to be used as materials for high-temperature applications. Short-fiber metal matrix composites are particularly interesting and significant among other composites, due to their comparatively low cost and ease of machining into complex shapes.

Since the creep tests are usually expensive and very time consuming and also suffer some difficulties and limitations, analytical and numerical investigations are carried out to replace experimental tests by analytical or numerical simulations. The related previous studies can be classified into three categories (analytical, experimental, and numerical). Various consequential analytical [1–16], experimental [17–23] as well as numerical [24–29] investigations have been conducted in the field of composites' creep and its applications.

The previous analytical researches are usually based on the shear-lag models [1–6]. A one-dimensional shear-lag model was originally presented by Cox [1]; this was a comprehensive and powerful method for stress transfer analyses of unidirectional fibrous composites. In this way, some researchers have used an imaginary fiber technique for analyzing stress transfer in the fiber and in the matrix [3,5–8]. In most of the previous researches, the fiber and the matrix behave elastically during

* Corresponding author at: Islamic Azad University of Zanjan, Eetemadieh, Shahid mansoory .st, 45156-58145 Zanjan, Iran. Tel.: +982414260063; fax: +982414260063.
E-mail addresses: mondali@srbiau.ac.ir (M. Mondali), vahid.monfared@azu.ac.ir (V. Monfared), Abedian@sharif.edu (A. Abedian).

1631-0721/$ – see front matter
http://dx.doi.org/10.1016/j.crme.2013.04.004

stress analysis. Recently, Mondali et al. [6] presented an analytical model for obtaining a steady-state creep deformation and stress analysis of composites with elastic short fibers using the shear-lag theory and the imaginary fiber technique, where the creep behavior of matrix was also considered to follow an exponential law. Also, the high-temperature creep behavior of short-fiber-reinforced ceramic-matrix composites has been studied based on the advanced shear-lag theory, considering a power-law creep for both matrix and fiber under uniaxial loading [7]. In this research, a parametric study was undertaken to define the effects of the fiber volume fraction and the fiber/matrix interface sliding factor on the composite's creep rate. Jiang et al. [8] presented an analytical model for three-dimensional elastic stress field distribution in short-fiber composites under axial loading and thermal residual stresses using the imaginary fiber technique, equilibrium and compatibility conditions. Moreover, other analytical methods have been presented based on analogies to perfect plasticity [9], phenomenological analysis [10], viscoelastic creep [11], continuum model [12], potential function [13], variational procedure [14], complex variable method [15], and, recently, dimensionless parameter and mapping function techniques [16]. For instance, a general formulation based on analogies to perfect plasticity has been analytically presented for the constitutive equations in the steady-state creep of an element with anisotropic material under multi-axial stress states by Berman and Pai [9]. Also, phenomenological analysis has been used by De Silva [10] to investigate the creep mechanism in a fiber composite using virtual displacements. Also, primary creep deformation of a unidirectional metal matrix composite based on the continuum model has been studied analytically by Min and Crossman [12]. Besides, a variational procedure has been proposed for estimating the effective constitutive behavior of polycrystalline materials undergoing high-temperature creep [14].

Experimental investigations are usually necessary for obtaining the creep and elastic properties of the short-fiber composites. Creep behavior of Kevlar 49/ERLA 4617 epoxy composites at room temperature has been studied experimentally [18]. Assessment of the creep rate in lead specimens containing aligned rods of phosphor bronze has been done by A. Kelly and K.N. Street [17]. Moreover, some authors have studied the steady-state creep behavior of short-fiber metal matrix composites [19–22]. Morimoto et al. [20] have analyzed the steady-state creep behavior of the Al6061/SiC composite at 573 K. Aluminum matrix composites with planar-random graphite fibers and SiC whiskers have been evaluated for their high-temperature performances [21]. The effect of the occurrence of the creep phenomenon during aging has been analyzed in polyurethane thermoplastic during aging at 70 °C and at 90 °C [23].

Numerical analyses and tests have also been performed in metal matrix composites [24,26,28,29]. For example, Park and Holmes [25] developed two- and three-dimensional FEM models to analyze the tensile creep and creep-recovery behavior of unidirectional fiber-reinforced ceramic composites. The fiber–matrix interlayer creep characteristics in indentation creep tests were numerically investigated using a creep finite element analysis by Yue and Lu [27]. Also, Ghavami et al. [29] presented a numerical finite difference approach to obtain the steady-state creep stress and displacement rate fields of the Al6061/15%SiC composite under both the perfect bond and the interfacial debonding assumptions. Moreover, essential and valuable formulations and theorems in plasticity and creep have been analyzed and reviewed in some references and books [30,31].

In experimental studies, some defects or failure arising from manufacturing processes establish the causes for inconsistency in predicted mechanical properties compared with numerical and analytical simulations. Note that simulating all defects such as the fiber misorientation, voids, cracks and other similar defects in numerical and analytical models is probably impossible. In most of the previous analytical researches, a number of assumptions and simplifications have been made, such as ignoring some equilibrium and constitutive equations and also assuming a linear behavior for the interfacial shear stress [6].

In the present work, a perfect fiber/matrix interface is assumed and the steady-state creep behavior of the matrix is described by an exponential law. Also, the incompressibility condition, the constitutive and equilibrium equations, and the boundary conditions are completely satisfied here. The new analytical model is proposed based on the shear-lag theory, the imaginary fiber technique, Hermite polynomials, hyperbolic trigonometric functions and power series. Note that the displacement rates on the top of the fiber (region II) are analytically obtained without considering any non-analytical assumption, unlike the prior studies [1–8]. The obtained analytical results are then validated by finite element modeling and the other available analytical approaches. For this purpose, the Al6061/15%SiC composite has been selected as a case study.

Finally, the presented method can be used for analyzing creep in nano-composites, visco-elasto-plastic problems and mechanical design under high temperature and stress because of its high performance in determination of all unknown parameters.

2. Material and method

2.1. Composite model

The unit cell model shown in Fig. 1 has been used by many investigators to model a short-fiber composite as representative of a composite reinforced with whiskers [3,5,6,8,20].

The volume fraction and aspect ratio of the fiber are $f = a^2 l / b^2 l'$ and $s = l/a$, respectively. Also, in this work, $k = l'a/lb$ is assumed as a parameter related to the unit cell geometry. The cylindrical polar coordinate system (r, θ, z) is employed for creep analysis. Also, elastic deformations are very small and are neglected compared with creep deformations. Fibers behave elastically during the analysis unlike the matrix, which follows a steady-state creep behavior. The second-stage creep behavior of the matrix is described by an exponential law (Eq. (1)):

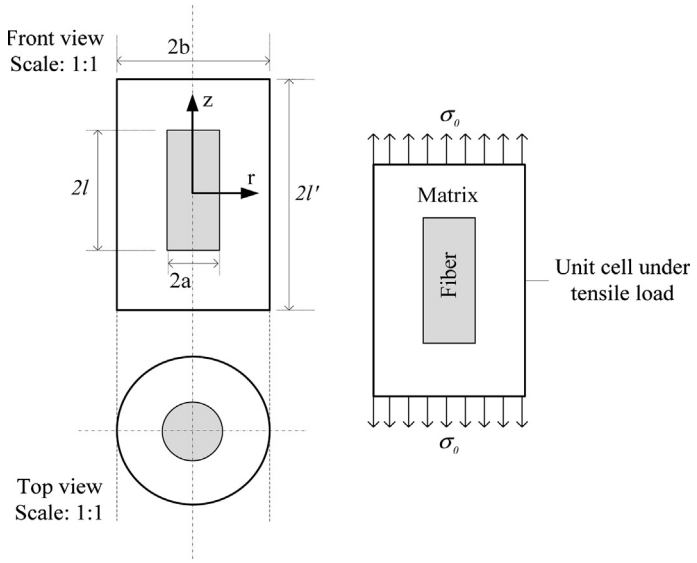

Fig. 1. Unit cell model.

$$\dot{\varepsilon}_{eq} = A \exp\left(\frac{\sigma_{eq}}{B}\right) \tag{1}$$

Parameters $\dot{\varepsilon}_{eq}$ and σ_{eq} are the equivalent strain rate and the equivalent stress, respectively. Also, A and B are material constants ruling steady-state creep. The mentioned parameters will be introduced in the following sections.

2.2. Formulations

The generalized constitutive equations for the creep small deformation of the matrix material are as the following [30,31]:

$$\dot{\varepsilon}_r = \psi\left[\sigma_r - \nu(\sigma_\theta + \sigma_z)\right] \tag{2a}$$
$$\dot{\varepsilon}_\theta = \psi\left[\sigma_\theta - \nu(\sigma_r + \sigma_z)\right] \tag{2b}$$
$$\dot{\varepsilon}_z = \psi\left[\sigma_z - \nu(\sigma_r + \sigma_\theta)\right] \tag{2c}$$
$$\dot{\gamma}_{rz} = 3\psi\tau_{rz} \tag{2d}$$

in which $\psi = \frac{\dot{\varepsilon}_e}{\sigma_e}$ and $\nu = \frac{1}{2}$. Solving Eqs. (2a)–(2d) gives:

$$\sigma_r + X = t \tag{3a}$$
$$\sigma_z + \Pi = t \tag{3b}$$
$$\sigma_\theta + \Gamma = t \tag{3c}$$
$$X = 4\tau_{rz}(\dot{\varepsilon}_r + 2\dot{\varepsilon}_\theta + 1.5\dot{\varepsilon}_z)\dot{\gamma}_{rz}^{-1} \tag{3d}$$
$$\Pi = 2\tau_{rz}(\dot{\varepsilon}_r + 2\dot{\varepsilon}_\theta)\dot{\gamma}_{rz}^{-1} \tag{3e}$$
$$\Gamma = 0 \tag{3f}$$

where t is a constant and $\dot{\gamma}_{rz}$ is the shear strain rate. Also, the incompressibility condition should be satisfied, that is:

$$\frac{\partial \dot{u}}{\partial r} + \frac{\dot{u}}{r} + \frac{\partial \dot{w}}{\partial z} = 0 \tag{4}$$

Parameters $\dot{u}$ and $\dot{w}$ are the radial and axial displacement rates, respectively. Also, the equivalent stress σ_{eq} and the equivalent strain rate $\dot{\varepsilon}_{eq}$ are given by:

$$\sigma_{eq} = \frac{\sqrt{2}}{2}\left[\frac{2}{3}\left(\frac{\sigma_{eq}\dot{\gamma}_{rz}}{\dot{\varepsilon}_{eq}}\right)^2 + (\sigma_r - \sigma_\theta)^2 + (\sigma_r - \sigma_z)^2 + (\sigma_z - \sigma_\theta)^2\right]^{\frac{1}{2}} \tag{5}$$

$$\dot{\varepsilon}_{eq} = \frac{\sqrt{2}}{3}\left[6\dot{\varepsilon}_{rz}^2 + (\dot{\varepsilon}_r - \dot{\varepsilon}_\theta)^2 + (\dot{\varepsilon}_r - \dot{\varepsilon}_z)^2 + (\dot{\varepsilon}_z - \dot{\varepsilon}_\theta)^2\right]^{\frac{1}{2}} \tag{6}$$

The equilibrium equations for the axisymmetric problem considering the cylindrical coordinates (r, θ, z) are:

$$\frac{\partial \sigma_z}{\partial z} + \frac{\partial \tau_{rz}}{\partial r} + \frac{\tau_{rz}}{r} = 0 \tag{7a}$$

$$\frac{\partial \sigma_r}{\partial r} + \frac{\partial \tau_{rz}}{\partial z} + \frac{\sigma_r - \sigma_\theta}{r} = 0 \tag{7b}$$

where $\dot{\varepsilon}_r$, $\dot{\varepsilon}_\theta$, $\dot{\varepsilon}_z$, and $\dot{\varepsilon}_{rz}$ are the strain rate components in the directions indicated by subscripts. Also, σ_r, σ_θ σ_z and τ_{rz} are the radial, circumferential, axial and shear stress components, respectively.

2.3. Boundary conditions

In order to determine and analyze the creep behavior, the following boundary conditions (BCs) are as follows.
(i) For the region I in the creeping matrix ($a < r < b$, $0 < z < l$):

$$\dot{u}(a,z)|_{0\leqslant z\leqslant l} = \dot{w}(a,z)|_{0\leqslant z\leqslant l} = \dot{w}(r,0)|_{a\leqslant r\leqslant b} = 0 \tag{8a}$$

$$\dot{w}(r,l)|_{a<r\leqslant b} = \frac{2l\dot{u}_b}{b}, \qquad \dot{w}(b,l) = \frac{2l\dot{u}_b}{b}, \qquad \dot{u}(b,z)|_{0\leqslant z\leqslant l} = \dot{u}_b \tag{8b}$$

$$\tau_{rz}(r,0)|_{a\leqslant r\leqslant b} = \tau_{rz}(b,z)|_{0\leqslant z\leqslant l} = 0 \tag{8c}$$

$$\dot{\gamma}_{rz}(r,0)|_{a\leqslant r\leqslant b} = \dot{\gamma}_{rz}(b,z)|_{0\leqslant z\leqslant l} = 0 \tag{8d}$$

$$\tau^m_{rz}(a,z)|_{0\leqslant z\leqslant l} = \tau^f_{rz}(a,z)|_{0\leqslant z\leqslant l} = \tau_i \tag{8e}$$

$$\sigma^m_r(a,z)|_{0\leqslant z\leqslant l} = \sigma^f_r(a,z)|_{0\leqslant z\leqslant l} = \sigma^m_\theta(a,z)|_{0\leqslant z\leqslant l} = \sigma^m_z(a,z)|_{0\leqslant z\leqslant l} \tag{8f}$$

(ii) For the region II in the creeping matrix ($0 < r < b, l < z < l'$):

$$\dot{u}'(0,z)|_{l\leqslant z\leqslant l'} = 0, \qquad \dot{w}'(r,l')\big|_{0\leqslant r\leqslant b} = \frac{2l'\dot{u}_b}{b}, \qquad \dot{u}'(b,z)|_{l\leqslant z\leqslant l'} = \dot{u}_b \tag{8g}$$

$$\tau_{rz}(0,z)|_{l\leqslant z\leqslant l'} = \tau_{rz}(r,l')\big|_{0\leqslant r\leqslant b} = \tau_{rz}(b,z)|_{l\leqslant z\leqslant l'} = 0 \tag{8h}$$

$$\dot{\gamma}_{rz}(0,z)|_{l\leqslant z\leqslant l'} = \dot{\gamma}_{rz}(r,l')\big|_{0\leqslant r\leqslant b} = \dot{\gamma}_{rz}(b,z)|_{l\leqslant z\leqslant l'} = 0 \tag{8i}$$

$$\dot{u}'(r,l)|_{a<r\leqslant b} = \dot{u}(r,l)|_{a<r\leqslant b}, \qquad \dot{w}'(r,l)|_{a<r\leqslant b} = \dot{w}(r,l)|_{a<r\leqslant b} = \frac{2l\dot{u}_b}{b} \tag{8j}$$

$$\dot{u}'(r,l)|_{0\leqslant r\leqslant a} = \dot{u}(r,l)|_{0\leqslant r\leqslant a} = \dot{w}'(r,l)|_{0\leqslant r\leqslant a} = \dot{w}(r,l)|_{0\leqslant r\leqslant a} = 0 \tag{8k}$$

$$\sigma_r(0,z)|_{l\leqslant z\leqslant l'} = \sigma_\theta(0,z)|_{l\leqslant z\leqslant l'}, \qquad \sigma_z(r,l')\big|_{0\leqslant r\leqslant b} = \sigma_0 \tag{8m}$$

For example, the boundary condition $\dot{w}'(r,l')|_{0\leqslant r\leqslant b} = 2l'\dot{u}_b/b$ is obtained by the incompressibility condition. Primed and unprimed signs denote respectively the regions II and I in the mentioned unit cell. Axial force equilibrium conditions between the matrix and the fiber at any z location in the direction of the model length are introduced by:

$$b^2\sigma_0 = a^2\bar{\sigma}^f_z + \left(b^2 - a^2\right)\bar{\sigma}^m_z \tag{9}$$

where the superscripts m and f denote the matrix and fiber and the bar sign on the stress symbol ($\bar{\sigma}^m_z$) denotes the average value over the cross-sections of the matrix and of the fiber (for simplicity in relations and formulations, some of them have not the superscript m, but the existence of the superscript f is necessary). It should be mentioned that all obtained results are related to the matrix in the steady-state creep of the short-fiber composites. The absence and presence of the superscript m indicate that the mentioned parameter is related to the matrix, but the presence of the superscript f is necessary for indicating the fiber. For instance, $\bar{\sigma}^m_z \cong \bar{\sigma}_z$, $\dot{u}(r,z) \cong \dot{u}^m(r,z)$. Deformed and undeformed edges of the unit cell are shown in Fig. 2 for the case of steady-state creep under tensile axial stress.

2.4. Problem solution steps

First, the radial and axial displacement rates $\dot{u}$ and $\dot{w}$ are obtained utilizing the incompressibility and appropriate boundary conditions. The radial displacement rate $\dot{u}$ is a combination of the orthogonal, hyperbolic trigonometric, well-behaved functions and power series (see Eqs. (10a) and (11a), (11b)). This combination results in an excellent and accurate prediction for the second-stage creep behavior. After obtaining the displacement rates, all strain rate components and shear stresses are determined considering one unknown $\dot{u}_b$ simply (see Section 3).

Therefore, the radial displacement rate in the outer surface $\dot{u}_b$ should be determined (see Section 4). This parameter is obtained using the shear lag and the imaginary fiber technique, considering new displacement rates in region II (see Eqs. (17)–(24) and (8g)–(8m)). Finally, stress fields will be determined using constitutive and equilibrium equations, considering incompressibility and boundary conditions and geometric relations (Eqs. (1)–(9) and (12)–(16)). These steps are completely presented in the detailed explanations of the following sections.

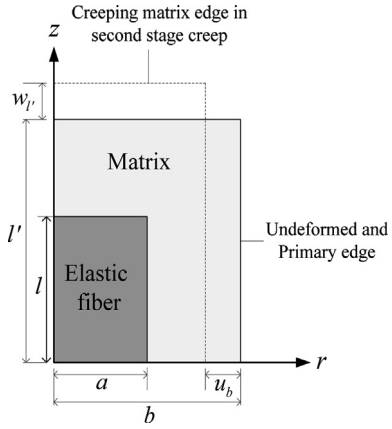

Fig. 2. Undeformed and crept edges.

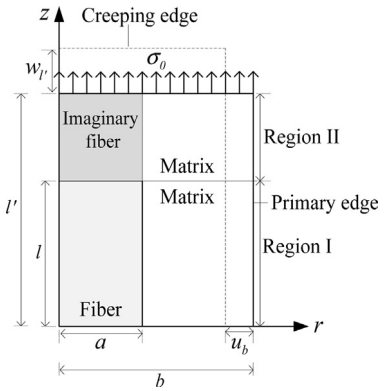

Fig. 3. Presentation of important regions in the unit cell for solving the creep problem.

3. Theory and calculations

Combination of the Hermite polynomials as a special function, hyperbolic trigonometric functions and power series is a powerful tool for predicting behavior of the unknowns. This can be another novelty of the present research, which provides exact results compared with FEM results. Hermite polynomials are called the classical orthogonal polynomials. These functions and polynomials behave well because of smooth changes in small intervals and smooth gradients. Radial and axial displacement rates $\dot{u}(r,z)$ and $\dot{w}(r,z)$ should satisfy the boundary and incompressibility conditions. Here, the radial displacement rate $\dot{u}(r,z)$ is obtained by mathematical combination of the Hermite polynomials, of hyperbolic trigonometric functions and of power series. Then, the coupled displacement rate $\dot{w}(r,z)$ is determined by the incompressibility condition in the creeping matrix in region I (see Fig. 3).

Hermite polynomials $H_n(r)$ and hyperbolic trigonometric function $HTF_n(r)$ considering power series $PS_n(r)$ for obtaining the steady-state creep behavior of the creeping matrix are given below:

$$\dot{u}(r,z) = k_1 H_n(r) + k_2 HTF_n(r) + PS_n(r) \tag{10a}$$

in which the hyperbolic trigonometric function $HTF_n(r)$ and $HTF_\infty(r)$ are given as:

$$HTF_n(r) = \sum_{k=0}^{n} \frac{r^{2k+1}}{(2k+1)!} = r\prod_{k=1}^{n}\left(1+\frac{r^2}{k^2\pi^2}\right) \tag{10b}$$

$$HTF_\infty(r) = \sum_{k=0}^{\infty} \frac{r^{2k+1}}{(2k+1)!} = r\prod_{k=1}^{\infty}\left(1+\frac{r^2}{k^2\pi^2}\right) = \sinh(r) \tag{10c}$$

Also, Hermite polynomials $H_n(r)$ are in the form:

$$H_n(r) = (-1)^{\frac{n}{2}} n! \sum_{k=0}^{\frac{n}{2}} (-1)^k \frac{(2r)^{2k}}{(2k)!(\frac{n}{2}-k)!}, \quad \text{if } n \text{ even} \tag{10d}$$

$$H_n(r) = (-1)^{\frac{n-1}{2}} n! \sum_{k=0}^{\frac{n-1}{2}} (-1)^k \frac{(2r)^{2k+1}}{(2k+1)!(\frac{n-1}{2}-k)!}, \quad \text{if } n \text{ odd} \tag{10e}$$

Power series $PS_n(r)$ is given as:

$$PS_n(r) = \sum_{k=0}^{n} a_k r^k \tag{10f}$$

$H_n(r)$ is the Hermite polynomial of degree n. The axial displacement rate $\dot{w}(r,z)$ is obtained by the incompressibility condition and writes:

$$\dot{w}(r,z) = -\left[(-1)^{\frac{n}{2}} n! k_1 \sum_{k=0}^{\frac{n}{2}} (-1)^k \frac{(2k+1) r^{2k-1} 2^{2k}}{(2k)!(\frac{n}{2}-k)!} + k_2 \sum_{k=0}^{n} \frac{(k+1) 2r^{2k}}{(2k+1)!} + \sum_{k=0}^{n} a_k r^{k-1}(k+1) \right] z, \quad \text{if } n \text{ even} \tag{11a}$$

$$\dot{w}(r,z) = -\left[(-1)^{\frac{n-1}{2}} n! k_1 \sum_{k=0}^{\frac{n-1}{2}} (-1)^k \frac{(2k+3) 2^{2k} r^{2k}}{(2k+1)!(\frac{n-1}{2}-k)!} + k_2 \sum_{k=0}^{n} \frac{(k+1) 2r^{2k}}{(2k+1)!} + \sum_{k=0}^{n} a_k r^{k-1}(k+1) \right] z, \quad \text{if } n \text{ odd} \tag{11b}$$

Here, the unknown coefficients of k_i's and a_k's are also determined by the extended boundary conditions (BCs) presented in Eqs. (8a)–(8f). For example, these boundary conditions $\dot{w}(a,0) = \dot{w}(a,0.1l) = \dot{w}(a,0.2l) = \dot{w}(a,0.3l) = \cdots = \dot{w}(a,l) = 0$ are the extended boundary conditions for the boundary condition $\dot{w}(a,z)|_{0 \leqslant z \leqslant l} = 0$ in the creeping matrix in region I. In addition, the creep strain rate components $\dot{\varepsilon}_r$, $\dot{\varepsilon}_\theta$ and $\dot{\varepsilon}_z$ (Eqs. (12)–(15)) may be given by:

$$\dot{\varepsilon}_r = \frac{\partial \dot{u}}{\partial r} = (-1)^{\frac{n}{2}} n! k_1 \sum_{k=0}^{\frac{n}{2}} (-1)^k \frac{4k(2r)^{2k-1}}{(2k)!(\frac{n}{2}-k)!} + k_2 \sum_{k=0}^{n} \frac{(2k+1) r^{2k}}{(2k+1)!} + \sum_{k=0}^{n} k a_k r^{k-1}, \quad \text{if } n \text{ even} \tag{12a}$$

$$\dot{\varepsilon}_r = \frac{\partial \dot{u}}{\partial r} = (-1)^{\frac{n-1}{2}} n! k_1 \sum_{k=0}^{\frac{n-1}{2}} (-1)^k \frac{(2k+1)(2r)^{2k}}{(2k+1)!(\frac{n-1}{2}-k)!} + k_2 \sum_{k=0}^{n} \frac{(2k+1) r^{2k}}{(2k+1)!} + \sum_{k=0}^{n} k a_k r^{k-1}, \quad \text{if } n \text{ odd} \tag{12b}$$

The above equations (Eqs. (12a), (12b)) predict the radial strain rate behavior in the creeping matrix. Moreover, Eqs. (13a), (13b) define the circumferential strain rate in the creeping matrix as the following:

$$\dot{\varepsilon}_\theta = \frac{\dot{u}}{r} = (-1)^{\frac{n}{2}} n! k_1 \sum_{k=0}^{\frac{n}{2}} (-1)^k \frac{2^{2k} r^{2k-1}}{(2k)!(\frac{n}{2}-k)!} + k_2 \sum_{k=0}^{n} \frac{r^{2k}}{(2k+1)!} + \sum_{k=0}^{n} a_k r^{k-1}, \quad \text{if } n \text{ even} \tag{13a}$$

$$\dot{\varepsilon}_\theta = \frac{\dot{u}}{r} = (-1)^{\frac{n-1}{2}} n! k_1 \sum_{k=0}^{\frac{n-1}{2}} (-1)^k \frac{2^{2k+1} r^{2k}}{(2k+1)!(\frac{n-1}{2}-k)!} + k_2 \sum_{k=0}^{n} \frac{r^{2k}}{(2k+1)!} + \sum_{k=0}^{n} a_k r^{k-1}, \quad \text{if } n \text{ odd} \tag{13b}$$

Here, axial strain rates (Eqs. (14a), (14b)) write:

$$\dot{\varepsilon}_z = \frac{\partial \dot{w}}{\partial z} = -\left[(-1)^{\frac{n}{2}} n! k_1 \sum_{k=0}^{\frac{n}{2}} (-1)^k \frac{(2k+1) r^{2k-1} 2^{2k}}{(2k)!(\frac{n}{2}-k)!} + k_2 \sum_{k=0}^{n} \frac{(k+1) 2r^{2k}}{(2k+1)!} + \sum_{k=0}^{n} a_k r^{k-1}(k+1) \right], \quad \text{if } n \text{ even} \tag{14a}$$

$$\dot{\varepsilon}_z = \frac{\partial \dot{w}}{\partial z} = -\left[(-1)^{\frac{n-1}{2}} n! k_1 \sum_{k=0}^{\frac{n-1}{2}} (-1)^k \frac{(2k+3) 2^{2k} r^{2k}}{(2k+1)!(\frac{n-1}{2}-k)!} + k_2 \sum_{k=0}^{n} \frac{(k+1) 2r^{2k}}{(2k+1)!} + \sum_{k=0}^{n} a_k r^{k-1}(k+1) \right], \quad \text{if } n \text{ odd} \tag{14b}$$

In the above relations, $\dot{\varepsilon}_r$, $\dot{\varepsilon}_\theta$ and $\dot{\varepsilon}_z$ are the radial, circumferential and axial strain rates, respectively, only in the creeping matrix in the second-stage creep. In what follows, shear strain rates are given by:

$$\dot{\gamma}_{rz} = \frac{\partial \dot{u}}{\partial z} + \frac{\partial \dot{w}}{\partial r} = -\left[(-1)^{\frac{n}{2}} n! k_1 \sum_{k=0}^{\frac{n}{2}} (-1)^k \frac{(4k^2-1) r^{2k-2} 2^{2k}}{(2k)!(\frac{n}{2}-k)!} + k_2 \sum_{k=0}^{n} \frac{4k(k+1) r^{2k-1}}{(2k+1)!} \right.$$

$$+\sum_{k=0}^{n}\left(k^2-1\right)a_k r^{k-2}\Bigg]z, \quad \text{if } n \text{ even} \tag{15a}$$

$$\dot{\gamma}_{rz}=\frac{\partial \dot{u}}{\partial z}+\frac{\partial \dot{w}}{\partial r}=-\Bigg[(-1)^{\frac{n-1}{2}}n!k_1\sum_{k=0}^{\frac{n-1}{2}}(-1)^k\frac{k(2k+3)2^{2k+1}r^{2k-1}}{(2k+1)!(\frac{n-1}{2}-k)!}+k_2\sum_{k=0}^{n}\frac{4k(k+1)r^{2k-1}}{(2k+1)!}$$

$$+\sum_{k=0}^{n}\left(k^2-1\right)a_k r^{k-2}\Bigg]z, \quad \text{if } n \text{ odd} \tag{15b}$$

where $\dot{\gamma}_{rz}=2\dot{\varepsilon}_{rz}$. Parameter $\dot{\gamma}_{rz}$ has been assumed in previous researches [6], without any analytical reason, whereas this parameter is obtained analytically in this research (see Eqs. (15a), (15b)). The shear stress in the creeping matrix is obtained by Eqs. (1), (2a)–(2d), i.e.:

$$\tau_{rz}^{m}=\frac{B\ln(\frac{\dot{\varepsilon}_{\text{eq}}}{A})\dot{\gamma}_{rz}}{3\dot{\varepsilon}_{\text{eq}}} \tag{16}$$

The present method is only an approach based on the Hermite polynomials, hyperbolic trigonometric functions and power series (HHP). For the sake of creep analysis, the unit cell is divided into two separate regions I and II, shown in Fig. 3 ($\sigma_{\text{app}}=\sigma_0$).

It should be mentioned that accuracy and correctness of the results strongly depend on the boundary conditions and the displacement rate fields. Therefore, these boundary conditions and fields should be presented exactly.

4. Determination of $\bar{\sigma}_z^f$, $\dot{u}_b$ and other unknowns

In this section, the radial displacement rate in the outer surface $\dot{u}_b$ is obtained. Here, the rule of mixture, shear-lag theory, imaginary fiber technique and new displacement rates in region II $\dot{u}'(r,z)$ and $\dot{w}'(r,z)$ are used to determine this parameter. The following shear-lag theory has been introduced by Cox [1]:

$$\bar{\sigma}_z^f\big|_l^z=-\frac{2}{a}\int_l^z \tau_i(z)\,\mathrm{d}z, \quad \tau_i(z)=\tau_{rz}^{m}\big|_{r=a,0<z<l} \tag{17}$$

The determination of the shear stress in region II is similar to the method used analytically for region I with different displacement rates $\dot{u}'(r,z)$ and $\dot{w}'(r,z)$. The radial displacement rate in region II is given by:

$$\dot{u}'(r,z)=\sum_{i=\alpha}^{\beta}c_i r^{i\gamma}+\sum_{j=\beta+1}^{\theta}c_j(rz)^{j\eta}+\sum_{k=\theta+1}^{\Psi}c_k z^{k\lambda}+e^{k\Omega z}\ln(k\varphi r), \quad \Psi-\alpha\geqslant 75 \tag{18}$$

The axial displacement rate in the region II $\dot{w}'(r,z)$ is analytically determined using incompressibility conditions with consideration of Eqs. (4), (18); it yields:

$$\dot{w}'(r,z)=-z\sum_{i=\alpha}^{\beta}c_i r^{i\gamma-1}(i\gamma+1)-\sum_{j=\beta+1}^{\theta}\frac{c_j(1+\eta j)r^{j\eta-1}z^{j\eta+1}}{j\eta+1}-\sum_{k=\theta+1}^{\Psi}\frac{c_k z^{k\lambda+1}}{r(k\lambda+1)}+\frac{e^{k\Omega z}(1+\ln(k\varphi r))}{rk\Omega} \tag{19}$$

The coefficients of c_i's, c_j's and c_k's are obtained by suitable and extended boundary conditions (BCs) presented in Eqs. (8g)–(8m). According to Eq. (16), the shear stress in region II is obtained as:

$$\tau_i'(z)=\frac{B\ln(\dot{\varepsilon}'_{\text{eq}}/A)\dot{\gamma}'_{rz}}{3\dot{\varepsilon}'_{\text{eq}}}, \qquad \tau_i'(z)=\tau_{rz}^{m}\big|_{r=a,l<z<l'} \tag{20}$$

It should be mentioned that the shear stress $\tau_i'(z)$ has been assumed to be linear in region II, without analytical reason, in some references such as [6]. However, the shear stress $\tau_i'(z)$ is non-linear in region II. Introduction of Eqs. (18)–(20) is another novelty of this work on the steady-state creep of short-fiber composites. All primed parameters should be calculated again based on new displacement rates $\dot{u}'(r,z)$ and $\dot{w}'(r,z)$, considering the boundary conditions presented in Eqs. (8g)–(8m) analytically. The following equation is also obtained using the shear-lag equation, imaginary the fiber technique and new displacement rates $\dot{u}'(r,z)$ and $\dot{w}'(r,z)$ for region II:

$$\bar{\sigma}_z'^{f}\big|_l^{l'}=-\frac{2B}{3a}\int_l^{l'}\frac{\ln(\dot{\varepsilon}'_{\text{eq}}/A)\dot{\gamma}'_{rz}}{\dot{\varepsilon}'_{\text{eq}}}\,\mathrm{d}z \tag{21}$$

After substituting equivalent and shear strain rates into Eq. (21) and integrating, the average axial stress in the fiber can be obtained using the shear lag, the imaginary fiber technique and new displacement rates $\dot{u}'(r,z)$ and $\dot{w}'(r,z)$, considering $\bar{\sigma}_z'^f|_{z=l'} = \sigma_0 = \sigma_{app}$ and $\bar{\sigma}_z'^f|_{z=l} = \bar{\sigma}_z^f|_{z=l}$ in region II,

$$\bar{\sigma}_z^f = \frac{-blz}{2a}\left(\ln\left(1+\frac{\sqrt{6}\dot{u}_b z}{A}\right)-1\right)+\frac{Bl(l+l')}{\sqrt{3}a}-\frac{8\sqrt{3}l'}{3a}+\sigma_{app} \tag{22}$$

The only unknown parameter here is the radial displacement rate in the outer surface $\dot{u}_b$ which is calculated employing the rule of the mixture equation and the average value of stresses in r and z directions:

$$\frac{(1-\nu)}{l}\int_0^l \bar{\sigma}_z^f \,\mathrm{d}z + \nu B \ln\left(-\frac{2\dot{u}_b}{Ab}\right) = \sigma_0, \quad \nu = 1-f \tag{23}$$

Now, $\dot{u}_b$ is determined by Eq. (23), that is

$$\dot{u}_b = -A\exp\left(\frac{l'b\sigma_0\nu + fl - \sqrt{3}aB(b-a)}{l'Bb^2(b-a)^3}\right) \tag{24}$$

Stresses in the matrix, σ_z^m, σ_r^m and σ_θ^m are determined by solving equilibrium and constitutive equations, considering geometry relations. In accordance with this research and the obtained results, the following relations and boundary conditions can be used to obtain shear stresses in regions I and II:

$$\int_l^{l'} \tau_i'(z)\,\mathrm{d}z < \frac{1}{2}\tau_l\left(l-l'\right) \tag{25}$$

$$\tau_l l > \int_0^l \tau_i(z)\,\mathrm{d}z > \frac{1}{2}\tau_l l \tag{26}$$

$$\left.\frac{\partial\tau_i'}{\partial z}\right|_{z=l'} = 0, \qquad \left.\frac{\partial\tau_i'}{\partial z}\right|_{z=l} = \infty \tag{27}$$

Also, $\tau_i|_{z=l} = \tau_i'|_{z=l} = \tau_l = \tau_l'$ and $\tau_i'|_{z=l'} = \tau_i|_{z=0} = 0$ are boundary conditions related to steady-state creep in the creeping unit cell.

$$\left.\frac{\partial\tau_i}{\partial z}\right|_{z=0} = \infty, \qquad \left.\frac{\partial\tau_i}{\partial z}\right|_{z=l} = 0, \qquad \left.\frac{\partial^2\tau_i}{\partial z^2}\right|_{0<z<l} < 0, \qquad \left.\frac{\partial^2\tau_i'}{\partial z^2}\right|_{l<z<l'} > 0 \tag{28}$$

Moreover, the following relations can be employed for analyzing steady-state creep in the creeping short-fiber composite. As mentioned before, $\tau_i(z)$ and $\tau_i'(z)$ are shear stresses (at $r=a$) in regions I and II in the unit cell, respectively. The mentioned boundary conditions indicate that the gradients of shear stress curves in the fiber's end and in the middle of the fiber are respectively zero and infinity, due to the tensile steady-state creep of the short-fiber composite. Therefore, the smooth and mellow behavior of the steady-state creep is one of the important characteristics of the second-stage creep in the same regions of the unit cell:

$$\int_0^l \tau_i(z)\,\mathrm{d}z \cong 0.85\tau_l l \tag{29}$$

$$\int_l^{l'} \tau_i'(z)\,\mathrm{d}z \cong \frac{1}{3}\tau_l\left(l-l'\right) \tag{30}$$

$$\frac{1}{2}\tau_l l' \cong \int_0^l \tau_i(z)\,\mathrm{d}z + \int_l^{l'} \tau_i'(z)\,\mathrm{d}z \tag{31}$$

After determining the unknowns, results and discussions are presented in the following sections.

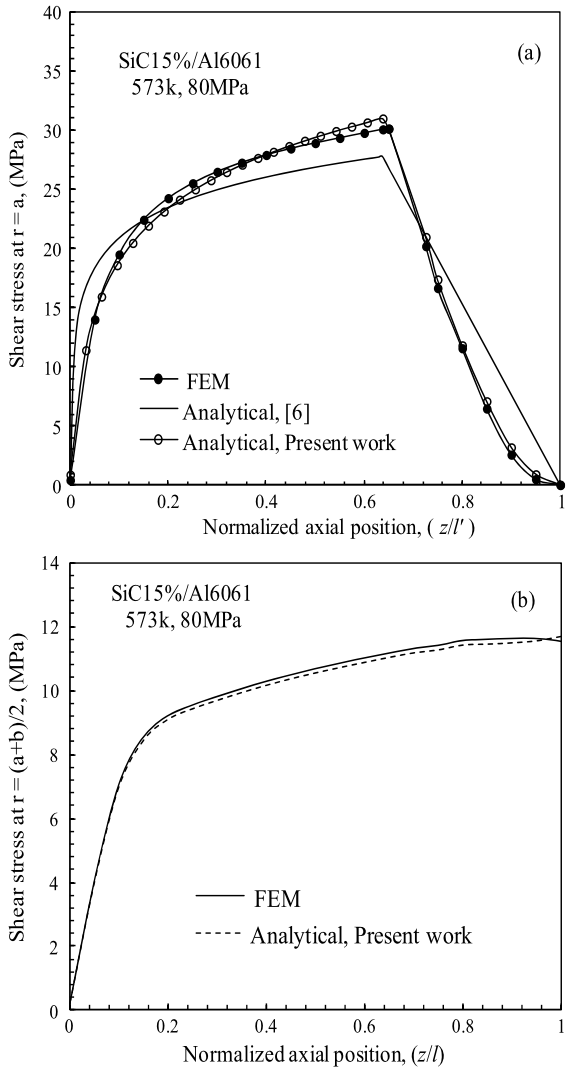

Fig. 4. Average shear stresses in the matrix at (a) $r = a$, $0 \leqslant z \leqslant l'$, (b) $r = (a + b)/2$, $0 \leqslant z \leqslant l$.

5. Results and discussions

To examine the validation of the present analytical model, the SiC/Al6061 composite is chosen as a test case. Afterward, the results obtained from the model are compared with the FEM results and also the previous analytical results by Mondali et al. [6]. FEM calculations will be carried out using the FE commercial code of ANSYS. The model geometry is chosen as shown in Fig. 1 and the surface conditions are applied as presented in Eqs. (8a)–(8m) (also see Figs. 2 and 3). Also, the axisymmetric non-linear quadratic element of PLANE 183 is used for FEM analysis. Results obtained from this study are shown in Figs. 4 and 5 and Tables 1–7 which are compared with the FEM, analytical, and available experimental results. For the composite used here (SiC/Al6061), the volume fraction of fibers is 15% and the fibers have an aspect ratio of 7.4 ($s = 7.4$) and $k = 0.76$, which is in accordance with the suggestions made by Morimoto et al. [20]. Also, the steady-state creep constants of the matrix material, A and B, in Eq. (1) are considered as $A = \exp(-24.7)$ and $B = 6.47$, values that had been given by Morimoto et al. [20]. The applied load and the temperature are considered to be $\sigma_0 = \sigma_{app} = 80$ MPa and $T = 300\,^{\circ}\mathrm{C}$, respectively.

According to Tables 1–6, good agreement is found among the stress components obtained by the mentioned methods. In comparison with the FEM, the results of the present model are more accurate than the other previously published results. Based on the obtained results, very high gradients are seen for the interfacial shear and equivalent stress behaviors at the middle regions of the fiber. However, very low gradients are observed for the interfacial shear and equivalent stress behaviors at the end of the fiber.

The logarithmic functions can interpret and explain the mentioned behaviors for the creeping matrix. Low and high gradients at the interface are arising from changes of the geometric factors, material properties, and applied loading.

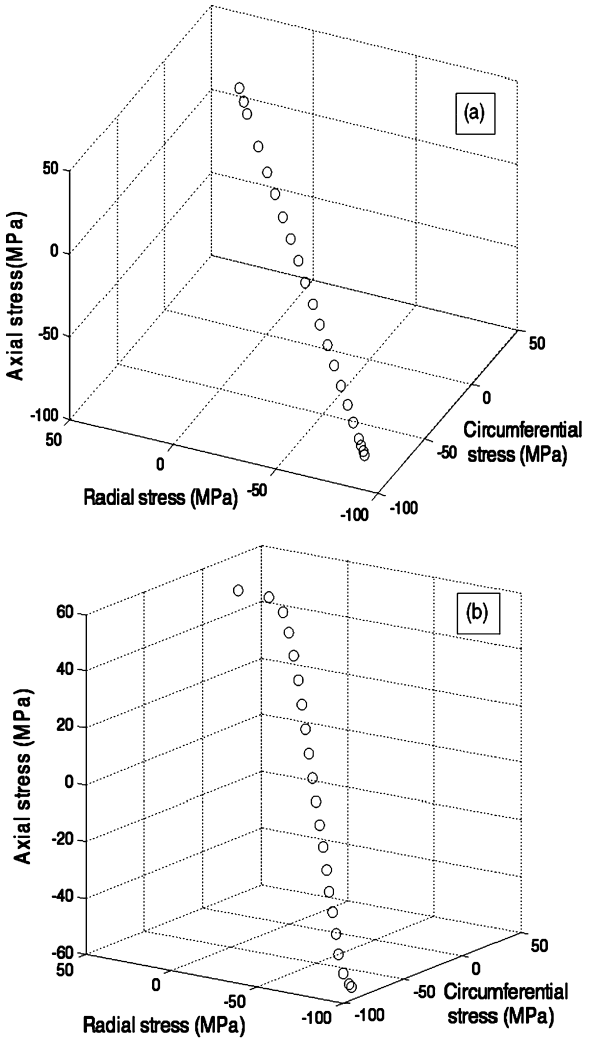

Fig. 5. Stresses relations for the creeping matrix in the region I at (a) $r = a$, (b) $r = b$.

However, linear behaviors are seen in the axial, radial and circumferential stress components at the interface and outer surface. Furthermore, gradient changes in the axial, radial and circumferential stresses are smooth and uniform. In accordance with the obtained results, interfacial shear and equivalent stresses have logarithmic and non-linear behaviors, whereas the axial, radial and circumferential stress behaviors are linear at the interface.

Figs. 4(a), 4(b) show the matrix shear stress predicted by the FEM and analytical methods at $r = a$, $0 \leqslant z \leqslant l'$ and $r = (a + b)/2$, $0 \leqslant z \leqslant l$. According to Fig. 4(a), the matrix shear stress is suddenly dropped near the end-region of the fiber (at region II: $l \leqslant z \leqslant l'$, $r = a$) due to a lack of the fiber and the proximity to the applied axial stress σ_0.

Smooth changes in gradient are observed in the shear stress curves in region I ($0 \leqslant z \leqslant l$, $r = a$, $(a + b)/2$) due to the existence of the fiber, away from the applied stress σ_0 in the mentioned region. In addition to the mentioned reasons, the matrix properties and geometric factors are also important and effective in the steady-state creep of the short-fiber composites.

The stress values are very high on the top of the fiber ($z = l$, $r = a$) due to a stress concentration effect, unlike the displacement rates. Also, high compressive stresses are seen in the middle of the unit cell at $z = 0$, due to tensile steady-state creep. Compressive radial stresses are establishing from the tensile creep of the matrix. Also, tensile creep of the matrix exerts very large compressive stresses to the fiber in the radial direction of the unit cell.

Figs. 5(a), 5(b) show the axial, radial and circumferential stress relations of the matrix in 3D space.

Table 7 presents the strain rate components normalized by the radial displacement rate at the outer surface of the unit cell.

Interestingly, good similarities and agreements are observed among our analytical and numerical results and the previously published analytical ones. In comparison with the other previous methods, that reported in the present work has

Table 1
Comparison of the analytical and FEM results for obtaining the shear and equivalent stresses in the matrix at $r = a$.

Methods	Stresses in the matrix (MPa)	Normalized axial position, $0 < z/l < 1$, $r = a$							
		0	0.13	0.27	0.4	0.54	0.67	0.81	1
Present work	Shear stress	0	18.4	22.6	25.1	26.9	28.3	29.4	30.7
	Equivalent stress	0	31.9	39.3	43.6	46.6	49.1	50.9	52.8
FEM	Shear stress	0	19.5	23.6	25.1	26.9	27.9	28.7	30.2
	Equivalent stress	0	33.27	40.3	44.7	46.9	49.3	50	51.9
Analytical, [6]	Shear stress	0	20.3	22.9	24.4	25.5	26.3	27	27.8
	Equivalent stress	0	35.2	39.7	42.3	44.2	45.6	46.8	48.2

Table 2
Comparison of the analytical and FEM results for obtaining the shear and equivalent stresses in the matrix at $r = b$.

Methods	Stresses in matrix (MPa)	Normalized axial position, $0 < z/l < 1$, $r = b$							
		0	0.13	0.27	0.4	0.54	0.67	0.81	1
Present work	Shear stress	0	0	0	0	0	0	0	0
	Equivalent stress	28.4	28.4	28.4	28.4	28.4	28.4	28.4	28.4
FEM	Shear stress	0	0	0	0	0	0	0	0
	Equivalent stress	28.9	28.5	28.7	28.7	28.6	28.6	28.5	24
Analytical, [6]	Shear stress	0	0	0	0	0	0	0	0
	Equivalent stress	29.3	29.3	29.3	29.3	29.3	29.3	29.3	29.3

Table 3
Comparison of the analytical and FEM results for obtaining the normal stresses in the matrix at $r = a$.

Stresses in matrix (MPa)	Normalized axial position, $0 < z/l < 1$, $r = a$							
	0	0.13	0.27	0.4	0.54	0.67	0.81	1
Axial, circumferential and radial stresses (present work)	−88.5	−82.09	−70.3	−54.8	−36.7	−17.4	1.6	25.5
Axial, circumferential and radial stresses (FEM)	−85.1	−83.2	−68.8	−54.2	−34.9	−16.3	−0.8	−383
Axial, circumferential and radial stresses (analytical, [6])	201.5	−78.6	−60.9	−43.5	−26.2	−8.7	8.7	33.5

Table 4
Comparison of the analytical and FEM results for obtaining the axial stress in the matrix at $r = b$.

Stresses in matrix (MPa)	Normalized axial position, $0 < z/l < 1$, $r = b$							
	0	0.13	0.27	0.4	0.54	0.67	0.81	1
Axial stress (analytical, present work)	−59.1	−50.1	−36.3	−19.4	−1.06	17.2	33.7	51.01
Axial stress (FEM)	−58.2	−52.6	−35.1	−19.7	−0.6	15.1	33	48.2
Axial stress (analytical, [6])	−84.4	−45.2	−28.3	−14.7	4.43	21.5	39.5	60.2

Table 5
Comparison of the analytical and FEM results for obtaining the radial stress in the matrix at $r = b$.

Stresses in matrix (MPa)	Normalized axial position, $0 < z/l < 1$, $r = b$							
	0	0.13	0.27	0.4	0.54	0.67	0.81	1
Radial stress (analytical, present work)	−94.8	−82.01	−67.3	−49.9	−31.9	−15.03	2.36	45.5
Radial stress (FEM)	−93.5	−82.6	−66.03	−50.4	−32.9	−14.2	3.07	46.9
Radial stress (analytical, [6])	−190.7	−75.9	−58.4	−41.3	−24.2	−7.03	10.3	34.9

Table 6
Comparison of the analytical and FEM results for obtaining the circumferential stress in the matrix at $r = b$.

Stresses in matrix (MPa)	Normalized axial position, $0 < z/l < 1$, $r = b$							
	0	0.13	0.27	0.4	0.54	0.67	0.81	1
Circumferential stress (analytical, present work)	−84.3	−75.25	−61.6	−45.04	−26.8	−8.6	8.2	26.5
Circumferential stress (FEM)	−82.9	−76.2	−60.8	−44.5	−27.5	−9.1	8.8	25.7
Circumferential stress (analytical, [6])	−182.6	−67.8	−50.3	−33.2	−16.1	1.08	18.4	43.03

Table 7
The strain rate values in the matrix normalized by $\dot{u}_b$ at the region I.

Normalized strain rates by $\dot{u}_b$	r		
	a	$1.5a$	b
$\dot{\varepsilon}_r/\dot{u}_b$	0	1	1.2
$\dot{\varepsilon}_\theta/\dot{u}_b$	0	0.2	0.5
$\dot{\varepsilon}_z/\dot{u}_b$	0	−1.3	−1.7
$\dot{\varepsilon}_{rz}/z\dot{u}_b$	−1.9	−0.7	0

high accuracy and simplicity, and also allows us to determine analytically the aforementioned unknowns, without any non-analytical assumption.

6. Conclusions

In the present research, a novel analytical model is presented based on Hermite polynomials, hyperbolic trigonometric functions and power series for analyzing the steady-state creep in the short-fiber composites under tensile axial load. An exponential creep law is considered to describe the steady-state creep behavior of the matrix in the unit cell; also, the fibers behave elastically. The analytical model is developed using the shear-lag theory, the imaginary fiber technique and also new proposed Hermite polynomials, hyperbolic trigonometric functions and power series, with considering the perfect bond condition at the interface. In summary,

- Combination of Hermite polynomials, hyperbolic trigonometric functions and power series is a suitable technique for creep analyzing. The results of the present analytical work are in good agreement with the FEM results compared to the other available previous results.
- The shear stress, displacement, and shear strain rates were determined in region II of the unit cell, without applying further assumptions. Considerable gradient changes are seen in the shear and equivalent stress behaviors, which are arising from nature of these parameters. Although the interfacial shear and equivalent stress behaviors are logarithmic, a linear behavior is observed in the axial, radial and circumferential stresses at the interface and the outer surface of the unit cell. The constant and smooth gradients are observed in the axial, radial and circumferential stress behaviors.
- The main advantage of the present method is its capability in predicting the stress fields, displacement and strain rate components in all regions of the composite. The method is also comprehensive and simple because it proposes the correct displacement rate fields.
- In comparison with previous analytical approaches, the results of the present work are closer to the FEM simulations. In addition, unlike in previous researches, all unknowns are determined without any non-analytical assumption in both regions I and II.
- Finally, this strong and comprehensive method can be used in various problems in applied physics and mechanics such as elastic and plastic analysis of nano-composites.

References

[1] H.L. Cox, The elasticity and strength of paper and other fibrous materials, Brit. J. Appl. Phys. 3 (1952) 72–79.
[2] A. Kelly, K.N. Street, Creep of discontinuous fibre composites. II. Theory for the steady-state, Proc. R. Soc. A 328 (1573) (1972) 283–293.
[3] C.H. Hsueh, R.J. Young, X. Yang, P.F. Becher, Stress transfer in a model composite containing a single embedded fiber, Acta Mater. 45 (4) (1997) 1469–1476.
[4] X.L. Gao, K. Li, A shear-lag for carbon nanotube-reinforced polymer composites, Int. J. Solids Struct. 42 (2005) 1649–1667.
[5] A. Abedian, M. Mondali, M. Pahlavanpour, Basic modifications in 3D micromechanical modeling of short fiber composites with bonded and debonded fiber end, Comput. Mater. Sci. 40 (2007) 421–433.
[6] M. Mondali, A. Abedian, A. Ghavami, A new analytical shear-lag based model for prediction of the steady-state creep deformations of some short-fiber composites, Mater. Design 30 (2009) 1075–1084.
[7] Y.R. Wang, T.W. Chou, Analytical modeling of creep behavior of short fiber reinforced ceramic matrix composites, J. Compos. Mater. 26 (9) (1992) 1269–1286.
[8] Z. Jiang, X. Liu, G. Li, J. Lian, A new analytical model for three-dimensional elastic stress field distribution in short fibre composite, Mater. Sci. Eng. A 366 (2004) 381–396.
[9] I. Berman, D.H. Pai, A theory of anisotropic steady-state creep, Int. J. Mech. Sci. 8 (5) (1966) 341–352.
[10] A.R.T. De Silva, A theoretical analysis of creep in fiber reinforced composites, J. Mech. Phys. Solids 16 (3) (1968) 169–186.
[11] N. Laws, R. McLaughlin, Self-consistent estimates for the viscoelastic creep compliances of composite materials, Proc. R. Soc. A 359 (1697) (1978) 251–273.
[12] B.K. Min, F.W. Crossman, Analysis of creep for metal matrix composites, J. Compos. Mater. 16 (3) (1982) 188–203.
[13] I. Chung, C.T. Sun, I.Y. Chang, Modeling creep in thermoplastic composites, J. Compos. Mater. 27 (10) (1993) 1009–1029.
[14] G. DeBotton, P. Ponte Castaneda, Variational estimates for the creep behaviour of polycrystals, Proc. R. Soc. A 448 (1932) (1995) 121–142.
[15] V. Monfared, M. Mondali, A. Abedian, Steady-state creep analysis of polymer matrix composites using complex variable method, J. Mech. Eng. Sci. (2013), http://dx.doi.org/10.1177/0954406212473391, in press.
[16] V. Monfared, M. Mondali, A. Abedian, Steady-state creep behavior of short-fiber composites by mapping, logarithmic functions (MF) and dimensionless parameter (DP) techniques, Arch. Civ. Mech. Eng. 12 (4) (2012) 455–463.
[17] A. Kelly, K.N. Street, Creep of discontinuous fibre composites. I. Experimental behaviour of lead-phosphor bronze, Proc. R. Soc. A 328 (1573) (1972) 267–282.

[18] R.H. Ericksen, Room temperature creep of Kevlar 49/epoxy composites, Composites 7 (3) (1976) 189–194.
[19] T.G. Nieh, Creep rupture of a silicon-carbide reinforced aluminum composite, Metall. Trans. A 15 (1984) 139–146.
[20] T. Morimoto, T. Yamaoka, H. Lilholt, M. Taya, Second stage creep of silicon carbide whisker/6061 aluminum composite at 573 K, J. Eng. Mater. Technol. 110 (1988) 70–76.
[21] R.B. Bhagat, M.F. Amateau, M.B. House, K.C. Meinert, P. Nisson, Elevated temperature strength, aging response and creep of aluminum matrix composites, J. Compos. Mater. 26 (11) (1992) 1578–1593.
[22] R. Fernandez, G. Gonzalez-Doncel, Threshold stress and load partitioning during creep of metal matrix composites, Acta Mater. 56 (2008) 2549–2562.
[23] A. Boubakri, N. Haddar, K. Elleuch, Y. Bienvenu, Influence of thermal aging on tensile and creep behavior of thermoplastic polyurethane, C. R. Mecanique 339 (10) (2011) 666–673.
[24] T.L. Dragon, W.D. Nix, Geometric factors affecting the internal stress distribution and high temperature creep rate of discontinuous fiber reinforced metals, Acta Metall. Mater. 38 (10) (1990) 1941–1953.
[25] Y.H. Park, J.W. Holmes, Finite element modeling of creep deformation in fibre-reinforced ceramic composites, J. Mater. Sci. 27 (23) (1992) 6341–6351.
[26] Y. Zhu-feng, Statistic modeling of the creep behavior of metal matrix composites based on finite element analysis, Appl. Math. Mech. 23 (4) (2002) 421–434.
[27] Z.F. Yue, Z.Z. Lu, A numerical determination of the fiber/matrix interlayer creep properties from the indentation creep testing in fiber reinforced composites, Mater. Sci. Eng. A 352 (1–2) (2003) 266–272.
[28] M. Mondali, A. Abedian, S. Adibnazari, FEM study of the second stage creep behavior of Al6061/SiC metal matrix composite, Comput. Mater. Sci. 34 (2005) 140–150.
[29] A. Ghavami, A. Abedian, M. Mondali, Finite difference solution of steady-state creep deformations in a short fiber composite in presence of fiber/matrix debonding, Mater. Design 31 (2010) 2616–2624.
[30] J.T. Boyle, J. Spence, Stress Analysis for Creep, Butterworth–Heinemann, Butterworth, Southampton, UK, 1983.
[31] J. Lubliner, Plasticity Theory, Dover Publications, United States, 2008.